

# Time-dependence Effects in Photospheric-Phase Type II Supernova Spectra

Luc Dessart\* and D. John Hillier†

\**Steward Observatory, The University of Arizona, Tucson, AZ 85721, USA*

†*Department of Physics and Astronomy, University of Pittsburgh, USA*

**Abstract.** We have incorporated time-dependent terms into the statistical and radiative equilibrium calculations of the non-LTE line-blanketed radiative transfer code CMFGEN. To illustrate the significant improvements in spectral fitting achieved for photospheric phase Type II SN, and to document the effects associated with time dependence, we model the outer  $6.1 M_{\odot}$  of ejecta of a BSG/RSG progenitor star. Hopping by 3-day increments, we compute the UV to near-IR spectral evolution for both continuum and lines, from the fully ionized conditions at one week to the partially recombined conditions at 6 weeks after the explosion. We confirm the importance of allowing for time-dependence in the modeling of Type-II SN, as recently discussed by Utrobin & Chugai for SN1987A. However unlike Utrobin & Chugai, who treated the radiation field in a core-halo approximation and assumed the Sobolev approximation for line formation, we allow for the full interaction between the radiation field and level populations, and study the effects on the full spectrum. At the hydrogen-recombination epoch, H I lines and Na D are considerably stronger and broader than in equivalent steady-state models, while Ca II is weakened. Former successes of steady-state CMFGEN models are unaffected, while former discrepancies are cured. Time dependence affects all lines, while the continuum, from the UV to the optical, changes only moderately. We identify two key effects: First, time dependence together with the energy gain through changes in ionization and excitation lead to an over-ionization in the vicinity of the photosphere, dramatically affecting line optical depths and profiles. Second, the ionization is frozen-in at large radii/velocities. This stems solely from the time-scale contrast between recombination and expansion and will occur, modulo non-thermal excitation effects, in all SN types. The importance of this effect on spectral analyses, across SN types and epochs, remains to be determined.

## INTRODUCTION

Because of radiative cooling and the fast expansion of the exploding mantle of the progenitor massive star, photospheric-phase Type II supernova (SN) spectra evolve rapidly. At shock breakout the spectral energy distribution (SED) peaks in the far-UV and X-rays. Subsequently the SED centers in the UV, then in the optical, and later in the infrared until the object disappears altogether into oblivion after a few years. From a radiative transfer perspective, the cooling induces a recombination to lower ionization stages that impose a strong blanketing effect on the energy distribution. A few days after explosion, the UV/optical/IR spectrum shows a UV-dominant SED, with Balmer/Paschen lines of Hydrogen, He I 5875Å, He I 10830Å, N II 4600Å, N II 5400Å, and a few isolated resonance lines such as Mg II 2802Å and Al III 1859Å. About a week later, hydrogen recombination kicks in, tied to a sudden enhancement in line-blanketing due to the switch from Fe III to Fe II. Dessart and Hillier [1] successfully modeled these epochs in the evolution of SN1999em, using steady-state non-LTE CMFGEN

models, solar metallicity, and a power-law density decline with an exponent of ten. In particular, He I lines at early times were fitted without invoking any additional non-thermal excitation due to  $^{56}\text{Ni}$ , as required by Baron et al. [2] in their analysis of SN1993W. In Dessart and Hillier [1], the spectroscopic analysis deliberately focused on the first 40 days since at such an epoch, we encountered growing difficulties in reproducing  $\text{H}\alpha$ ,  $\text{H}\beta$ , and the near-IR Paschen lines [3]. While we could reproduce the overall SED very well, line profiles were sizably narrower than observed at late times, suggesting that line formation regions predicted by CMFGEN were confined to velocities/radii that were too small. CMFGEN failed to reproduce observations, despite all attempts, whenever hydrogen started recombining at and above the photosphere.

The  $\text{H}\alpha$  problem has not been clearly emphasized in the literature, where one can see a great disparity in model atmosphere assumptions and agreement between theoretical predictions and observations, but no direct links to physical/numerical issues. In the eighties and early nineties, the recognized importance of non-LTE effects confronted the strong limitations of computer technology, so that only a few species were treated in non-LTE (i.e., usually hydrogen and helium), while the metals responsible for line blanketing were treated in LTE. Eastman and Kirshner [4] followed this approach to model the first ten days of SN1987A, and thus did not encounter obvious difficulties with hydrogen lines. Schmutz et al. [5], using an approximate non-LTE technique, had, on the contrary, great difficulty reproducing any of the Balmer lines, suggesting clumping as the culprit. Höflich [6] reproduced the SN1987A spectral evolution and the hydrogen lines, over many months, using a large “turbulent” velocity. In the more sophisticated non-LTE CMFGEN [7, 8] models presented in Dessart and Hillier [1, DH06], we found that decreasing the turbulent velocity weakens line-blanketing effects and increased, although only modestly, the strength of hydrogen lines. However, beyond 40 days after explosion, this tuning had no longer any important influence on the hydrogen lines. The non-LTE model atmosphere code PHOENIX reproduces the Balmer lines well [2, 9], but this may stem from their adoption of non-thermal ionization/excitation due to  $^{56}\text{Ni}$  at the photosphere just a few days after explosion, in mass shells moving at  $\geq 10000 \text{ km s}^{-1}$  in SN1987A [9] or  $\sim 9000 \text{ km s}^{-1}$  in SN1993W [2]. Hydrodynamical simulations of core-collapse SN predict that  $^{56}\text{Ni}$  has velocities of at most  $\sim 4000 \text{ km s}^{-1}$ , the nickel fingers being strongly decelerated at the H/He interface [10, 11]. The magnitude of this disagreement extends far beyond the uncertainties of explosion models and suggests a genuine incompatibility.

Interestingly, H I lines remain strong for months in all Type II SN, e.g. the “peculiar” SN1987A, the “plateau” SN1999em, and the “low-luminosity” SN1999br. CMFGEN models computed for these objects were unable to reproduce Balmer lines after  $\sim 4$  days in SN1987A,  $\sim 40$  days in SN1999em, and  $\sim 20$  days in SN1999br, all coincident with hydrogen recombination in the outflow. These three SN boast very different envelope structures, ejecta velocities, and light curves. SN1999br even synthesized an order of magnitude less  $^{56}\text{Ni}$  than average [12]. The only common property between these objects, which is connected to the  $\text{H}\alpha$  problem, is the recombination of the ejecta to a lower ionization state at the corresponding epoch.

Recently, Utrobin and Chugai [13, UC05] proposed that the effect of time-dependence, and the energy associated with changes in ionization/excitation, lead to a strong  $\text{H}\alpha$  line profile in SN1987A during the recombination epoch. They also

found that barium lines were affected, and that, with their more consistent approach, BaII 6142Å could be fitted using the LMC metallicity value. The steady-state models of Mazzali et al. [14] supported instead an abundance enhancement of five. Time dependence has been invoked in the past by Fransson and Kozma [15] to explain the late-time light curve of SN1987A, and the theoretical study of Pinto and Eastman [16, 17] showed that time dependence *in the radiation field* had a critical impact on the radiative transfer in Type Ias. Pinto and Eastman [16, 17], however, treat the material in LTE, in other words, they neglect any non-LTE and time-dependent terms in the rate equations (i.e. they do not solve the rate equations), focusing instead on the time-dependent *diffusion* of photons through an optically thick Type Ia SN ejecta. Similarly, Kasen et al. [18] neglect such explicit time dependence in the rate equations, computing the ionization and excitation state of the medium in LTE. Thus, although there is at present growing interest in accounting for time dependence in the radiation field, the often-used expedient of LTE, to maintain CPU costs low, has forced the neglect of both non-LTE and time-dependence in the level populations. One exception to these time-dependent LTE approaches is the work of Höflich [19], who treats time-dependence in the rate equations but, to our knowledge, has not discussed the associated effects on Type II SN spectra. In the present and forthcoming studies, we investigate thoroughly the effects of time-dependence in the rate equations and their impact on inferred ejecta properties. Time dependence in the radiation field is accounted for by ensuring that the emergent light from the model matches the observed flux from the Type II SN, using SN1999em as our reference SN [1].

Here, we report the salient features of a *time-dependent* non-LTE CMFGEN simulation covering the evolution of a Type II SN from one to six weeks after core collapse. We confirm the results of UC05 that time-dependence induces an over-ionization of the recombining ejecta and that it solves the H $\alpha$  problem. However unlike UC05, we self-consistently solve the radiation transfer equation — the coupling between the level populations and the radiation field is calculated and fully allowed for. Our study of the full spectrum predicts that all lines are significantly affected. The ionization of the ejecta and its evolution are so strongly modified that we predict even HeI 10830Å many weeks after explosion. This feature has been observed [3, 20], but never understood, and epitomizes the difficulty of line identification, abundance determinations, and chemical stratification in SN ejecta. In the next section, we present our baseline model, before moving onto the presentation and discussion of our results.

## MODEL

CMFGEN [7, 8] solves the radiative transfer equation in the comoving frame, subject to the constraints of radiative and statistical equilibrium. It assumes spherical symmetry. No explicit time-dependence in the radiation field is considered, i.e. light propagates instantaneously and thus is not subject to travel-time delays [21], and we still ignore relativistic effects. Both affect the energy transport (luminosity) at depth [16, 17]. However, unlike the version of CMFGEN used in [8, 22, 1], we now include explicitly time dependence in the rate equations that are solved for level populations, as well as in the

energy equation by accounting for changes in ionization and excitation. Our treatment, which follows directly from Mihalas and Weibel Mihalas [23], will be presented in detail in a follow-up paper (Hillier & Dessart 2006, in prep.).

We adopt a different procedure to model SN spectra from that employed previously. Rather than modeling, at each time, the region in the vicinity of the photosphere (i.e., from  $\tau_{\text{Rosseland}}$  of 30), we model the time evolution of a larger portion of the ejecta. As a starting point for our baseline model, we mapped onto the CMFGEN grid an envelope with the following properties:  $R_0 = 2.524 \times 10^{14}$  cm ( $R_0$  is the base radius),  $v_0 = 3470$  km s $^{-1}$  ( $v_0$  is the base velocity),  $R_0^3 \rho_0 = 6.781 \times 10^{33}$  g ( $\rho_0$  is the base density),  $\rho(r) = \rho_0 (R_0/r)^{10}$  ( $r$  is the radius), and  $L_0 = 3.6 \times 10^{11} L_\odot$  ( $L_0$  is the base luminosity). The maximum radius is 16 times the value of the base radius  $R_0$ . These initial conditions correspond to a base Rosseland optical depth of 4000, a total mass of  $6.1 M_\odot$ , and, assuming homology, a time after explosion of 8.4 days. We adopt a fixed composition, i.e. chemical homogeneity, with values consistent with the red-sugergiant progenitor of SN1999em [1, 24]. Adopted abundances, given by number, are: H/He = 5, C/He = 0.00017, N/He = 0.0068, O/He = 0.0001, and all metal species are at the solar value. Compared to the model atom used in DH06, we omit Cl, neon, aluminium, sulfur, chromium, manganese, and cobalt.

An initial steady-state model is then computed with the above parameters and it gives a spectrum that fits the observations of SN1999em at 7 days after explosion [8, Fig. 1], with a *fully-ionized* ejecta, little blanketing in the UV, and a dominance of hydrogen Balmer lines and HeI 5875Å in the optical range. We then hop in time by steps of  $\Delta t = 3$  days, i.e., all mass shells  $m$  in the initial model are evolved from their position  $r(m)$  to a new radius  $r'(m)$ , with  $r'(m) = r(m) + v_0(m)\Delta t$ , a new density  $\rho' = \rho(r/r')^3$ , but the same velocity. In practice, for each new model, CMFGEN adapts its 80-point grid to cover each optical-depth decade with at least five points.

The luminosity, set at the base, is adjusted at each epoch so that the *emergent* luminosity matches the inferred values for SN1999em (DH06), i.e. from  $\sim 10^9 L_\odot$  one week to  $\sim 10^8 L_\odot$  50 days after explosion. Despite the fixed composition at all times and the neglect of Cl, both of which affecting the late time appearance of Type II spectra (DH06) we support our thesis by showing in the next section a *representative* match between the spectrum of our baseline model and the optical observations of SN1999em. Detailed analyzes will be presented in a future paper.

## RESULTS AND DISCUSSION

To highlight the salient features of time-dependent CMFGEN models, we select the last baseline model computed in the sequence, corresponding to 48.7 days after explosion, and compare its properties to the same model, but computed by assuming steady-state. Fig. 1 shows the radial variation of the ionization fraction of hydrogen and helium for the time-dependent and steady-state models (left and middle panels). Time dependence systematically reduces the effective recombination rates, with the greatest effect occurring away from the photosphere where the densities are lowest and the velocities highest. In those regions and at 48.7 days, the ejecta preserves the high ionization it had at the start

of the time sequence, at  $\sim 8$  days after explosion, exhibiting the prevalence of ionized hydrogen and helium. Many other species are also affected, often showing comparable ionization profiles (i.e., a reduction of their degree of ionization near the photosphere and a growth of their degree of ionization at larger distances). Further, because of the enhanced H ionization, the electron density does not fall as steeply in the time-dependent CMFGEN model (Fig. 1). The electron temperature is strongly affected in the optically-thick layers, which remain hotter due to the reduced radiative cooling efficiency in the time-dependent case.

Thus, the effect of time dependence modifies the optical-depth of both continua and lines. The former occurs since more free electrons are available to scatter continuum photons. Further, certain ions are “over-abundant” by several orders of magnitude compared to the steady-state model. In the top panel of Fig. 3, although not tailored specifically to match an observation, the reddened ( $E(B - V) = 0.1$ ) spectrum of our baseline model (black) is overlaid on the optical spectrum of SN1999em observed on the 5th of Dec 1999 [25, blue], i.e.  $\sim 45$  days after explosion (DH06). Note the strong  $H\alpha$  line in this time-dependent CMFGEN synthetic spectrum, in agreement with the observation. In the lower panels, we present synthetic UV, optical, and near-IR spectra for the time-dependent and steady-state (red) CMFGEN models, normalized at  $12000\text{\AA}$ . To highlight the effect on individual species, we also compare synthetic spectra computed by allowing all continuum processes, but accounting only for bound-bound transitions of FeII and HI. Note the large effect on Balmer and Paschen lines, which appear stronger in both absorption and emission and are broader. FeII lines are stronger in the steady state model — stronger in absorption in the UV and stronger in emission in the optical. Similarly, in the lower panel, we zoom in on specific synthetic lines, accounting only for bound-bound transitions of NaI, CaII, or HeI.

In the time-dependent case, NaI  $5895\text{\AA}$  strengthens and broadens. This occurs because  $\text{Na}^+$  is the dominant ionization state in both models, but the increased electron density in the time-dependent model leads to an increase in the neutral Na fraction. Conversely, CaII  $8500\text{\AA}$  weakens, primarily because the relative fractions of  $\text{Ca}^+$  and  $\text{Ca}^{++}$  change significantly. HeI  $1.083\ \mu\text{m}$  is present only in the time-dependent case, as a broad flat-topped profile (overlapping with  $P\gamma$  in the full spectrum; top panel of Fig. 3), with a blue absorption maximum at  $1.038\ \mu\text{m}$  (equivalent to  $-13000\ \text{km s}^{-1}$ ).

The implications of time dependence are numerous and far reaching. We find that the effects of time dependence on level populations and on the energy budget allow the best of two worlds. Previous successes of CMFGEN at fitting the overall spectral energy distribution of photospheric phase Type II SN are left unchanged. The outstanding problem of the  $H\alpha$  line strength and the overall line profile widths are however solved. We, thus, confirm the importance of time-dependence effects, as suggested by UC05, even at early times. This provides a more physical and less dramatic explanation of the apparent ionization/excitation seen in photospheric-phase Type II SN spectra than invoking non-thermal ionization/excitation by  $^{56}\text{Ni}/^{56}\text{Co}$  in ejecta regions moving sometimes at  $\sim 10000\ \text{km s}^{-1}$ .

The change in ionization is large. Time dependence affects line profiles in a way that can mimic changes in chemical abundance in steady-state models, with dire consequences on the quantitative assessment of the chemical composition of SN outflows. Even more extreme is the case of HeI, absent in our steady state models after  $\sim 2$  weeks,

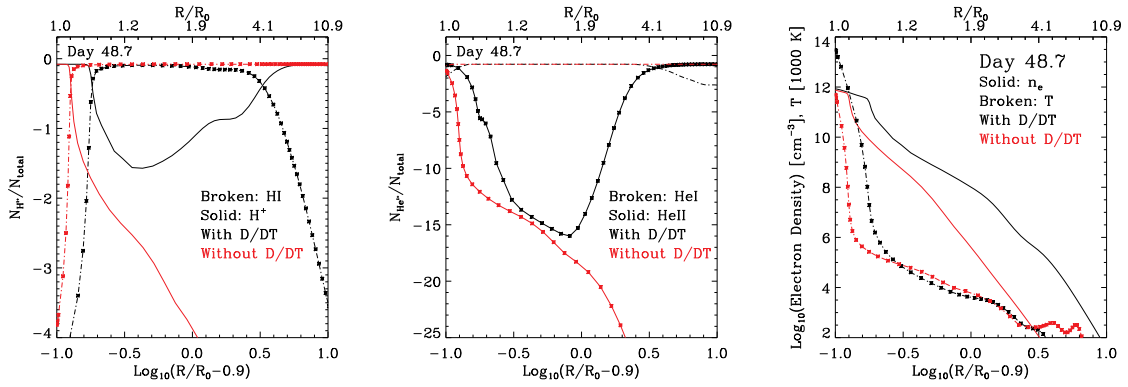


**FIGURE 1.** *Left:* Radial variation of the ionization fraction of Hydrogen (HII: solid line; HI: Broken line) for the models with time-dependence (black) and without (red), and at 48.7 days after explosion, but otherwise having *identical* parameters. Note the overionization of hydrogen at large radii, not present in its neutral state despite the very late time, akin to a frozen-in ionization. Symbols give the positions of the CMFGEN adaptive-grid points, for each model but for only one curve. Note the presence of the well-resolved recombination front near the base, deeper in for the steady-state CMFGEN model. *Middle:* Same as left, but for the ionization fraction of helium (HeII: solid line; HeI: Broken line). *Right:* Same as left, but for electron density and temperature.

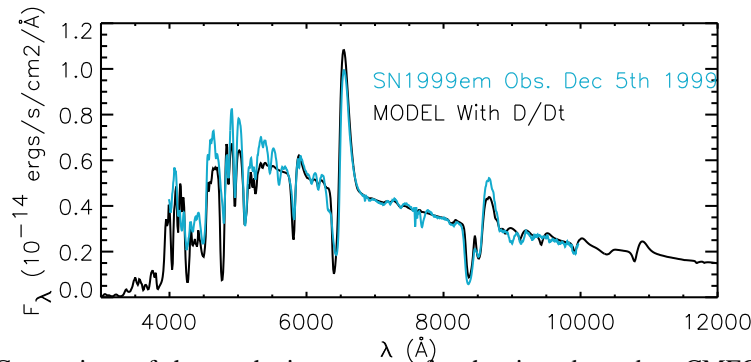


**FIGURE 2.** Comparison of the synthetic spectrum for the time-dependent CMFGEN model (black curve) at 48.7 days after explosion with Keck observations of SN1999em [25] on Dec. 5th 1999 (turquoise curve), at  $\sim 45$  days after explosion (DH06). The model has been reddened with  $E(B - V) = 0.1$ .

but present in equivalent time-dependent models even after 6 weeks, without any enhancement in abundance from the initial red-supergiant composition. An unidentified feature at  $1.03\mu\text{m}$  was observed by Hamuy et al. [3] in SN1999em at 4 weeks after explosion but not reproduced by DH06 with steady-state CMFGEN models; with time dependence effects, it can now be identified as HeI  $1.083\mu\text{m}$ . It also seems to be present in SN1987A a few weeks after the explosion [20]. It has been inferred in Type Ib/c SN [26], produced by non-thermal excitation [27], and even suggested in Type Ia SN [28], although MgII is expected to contribute, perhaps dominantly, to the feature [29]. In the future, we will investigate to what extent time dependence can be distinguished from non-thermal excitation, and if, together with the accurate treatment of non-LTE effects, they can help resolve the issue of the presence of helium in SN spectra.

Our investigation suggests that to model the emergent light from a SN at a given

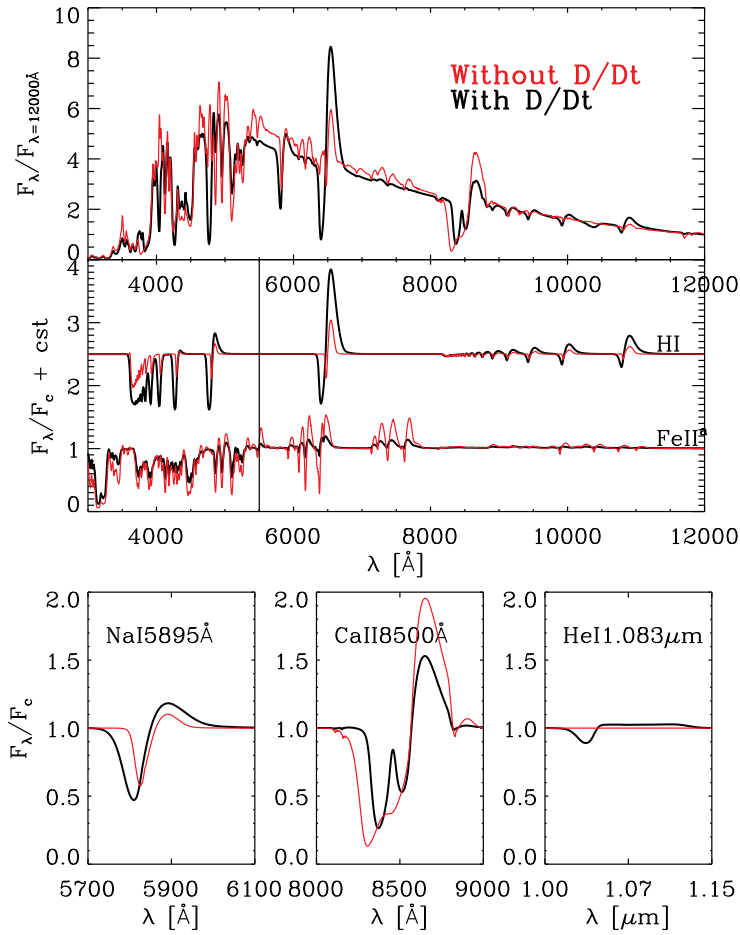


**FIGURE 3.** *Top:* Comparison of the synthetic spectra for the time-dependent CMFGEN model (black curve) and the equivalent steady-state CMFGEN model (red curve), both at 48.7 days after explosion. Accounting for time dependence leads to a comparatively higher ionization in the ejecta, sustained line optical depth at large radii/velocities, epitomized by H $\alpha$ . *Middle:* Rectified spectra (shifted vertically) obtained by accounting solely for bound-bound transitions of FeII (lower curves; line spectrum magnified by a factor of four beyond 5500Å for better rendering) and HI (upper curves). *Bottom:* Same as above, but this time zooming-in on specific spectral regions, i.e., NaI 5895Å (left), CaII 8500Å (middle), and HeI 1.083 $\mu$ m (right).

time, one needs to have the knowledge of the physical conditions in the SN envelope at previous times, all the way to the epoch when the ejecta was fully ionized. This calls for a change of strategy in SN spectroscopic modeling, and casts doubt on results using approaches that ignore the history of the SN ejecta. While the energy gain through hydrogen recombination in the outflow is a feature of Type II SN ejecta only, the frozen-in ionization at large distances/velocities stems from the order-of-magnitude larger recombination time-scale compared to expansion time-scale. This fact is not influenced by the energetics of recombination — it merely demonstrates that SN ejecta are so

tenuous and so fast that the ionization balance can be considerably affected by time dependence. This phenomenon should be a ubiquitous feature of SN ejecta and, at the very least, deserves considerably more attention that it has so far received.

Accounting for time dependence in CMFGEN opens new horizons. In particular, it is now sensible to model Type II SN throughout the photospheric phase. We will incorporate in CMFGEN the energy deposition due to unstable isotopes, to cover the nebular phase, and investigate a wider range of SN explosions, from core-collapse to thermonuclear runaways. We will also include relativistic effects, and time dependence for the radiation transport, to improve the energy transport at depth. We will finally assess the effects of time dependence on the correction factors used in the Expanding Photosphere Method [22].

## REFERENCES

1. L. Dessart, and D. J. Hillier, *A&A* **447**, 691–707 (2006), [astro-ph/0510526](#).
2. E. Baron, P. E. Nugent, D. Branch, P. H. Hauschildt, M. Turatto, and E. Cappellaro, *ApJ* **586**, 1199–1210 (2003), [astro-ph/0212071](#).
3. M. Hamuy, P. A. Pinto, J. Maza, N. B. Suntzeff, M. M. Phillips, R. G. Eastman, R. C. Smith, C. J. Corbally, D. Burstein, Y. Li, V. Ivanov, A. Moro-Martin, L. G. Strolger, R. E. de Souza, S. dos Anjos, E. M. Green, T. E. Pickering, L. González, R. Antezana, M. Wischnjewsky, G. Galaz, M. Roth, S. E. Persson, and R. A. Schommer, *ApJ* **558**, 615–642 (2001), [astro-ph/0105006](#).
4. R. G. Eastman, and R. P. Kirshner, *ApJ* **347**, 771–793 (1989).
5. W. Schmutz, D. C. Abbott, R. S. Russell, W.-R. Hamann, and U. Wessolowski, *ApJ* **355**, 255–270 (1990).
6. P. Höflich, *Proceedings of the Astronomical Society of Australia* **7**, 434–442 (1988).
7. D. J. Hillier, and D. L. Miller, *ApJ* **496**, 407–+ (1998).
8. L. Dessart, and D. J. Hillier, *A&A* **437**, 667–685 (2005), [astro-ph/0504028](#).
9. R. C. Mitchell, E. Baron, D. Branch, P. Lundqvist, S. Blinnikov, P. H. Hauschildt, and C. S. J. Pun, *ApJ* **556**, 979–986 (2001), [astro-ph/0104148](#).
10. K. Kifonidis, T. Plewa, H.-T. Janka, and E. Müller, *ApJL* **531**, L123–L126 (2000), [astro-ph/9911183](#).
11. K. Kifonidis, T. Plewa, H.-T. Janka, and E. Müller, *A&A* **408**, 621–649 (2003), [astro-ph/0302239](#).
12. A. Pastorello, L. Zampieri, M. Turatto, E. Cappellaro, W. P. S. Meikle, S. Benetti, D. Branch, E. Baron, F. Patat, M. Armstrong, G. Altavilla, M. Salvo, and M. Riello, *MNRAS* **347**, 74–94 (2004), [astro-ph/0309264](#).
13. V. P. Utrobin, and N. N. Chugai, *A&A* **441**, 271–281 (2005), [astro-ph/0501036](#).
14. P. A. Mazzali, L. B. Lucy, and K. Butler, *A&A* **258**, 399–411 (1992).
15. C. Fransson, and C. Kozma, *ApJL* **408**, L25–L28 (1993).
16. P. A. Pinto, and R. G. Eastman, *ApJ* **530**, 744–756 (2000).
17. P. A. Pinto, and R. G. Eastman, *ApJ* **530**, 757–776 (2000).
18. D. Kasen, R. C. Thomas, and P. Nugent, *ApJ* **383**, 308–313 (2006), [astro-ph/0606111](#).
19. P. Höflich, “ALI in Rapidly Expanding Envelopes,” in *ASP Conf. Ser. 288: Stellar Atmosphere Modeling*, edited by I. Hubeny, D. Mihalas, and K. Werner, 2003, pp. 185–+.
20. J. Spyromilio, R. A. Stathakis, R. D. Cannon, L. Waterman, W. J. Couch, and M. A. Dopita, *MNRAS* **248**, 465–478 (1991).
21. L. Ensmann, and A. Burrows, *ApJ* **393**, 742–755 (1992).
22. L. Dessart, and D. J. Hillier, *A&A* **439**, 671–685 (2005), [astro-ph/0505465](#).
23. D. Mihalas, and B. Weibel Mihalas, *Foundations of radiation hydrodynamics*, New York: Oxford University Press, 1984, 1984.
24. S. J. Smartt, G. F. Gilmore, C. A. Tout, and S. T. Hodgkin, *ApJ* **565**, 1089–1100 (2002), [astro-ph/0107499](#).



25. D. C. Leonard, A. V. Filippenko, E. L. Gates, W. Li, R. G. Eastman, A. J. Barth, S. J. Bus, R. Chornock, A. L. Coil, S. Frink, C. A. Grady, A. W. Harris, M. A. Malkan, T. Matheson, A. Quirrenbach, and R. R. Treffers, *PASP* **114**, 35–64 (2002), [astro-ph/0109535](#).
26. M. Hamuy, J. Maza, P. A. Pinto, M. M. Phillips, N. B. Suntzeff, R. D. Blum, K. A. G. Olsen, D. J. Pinfield, V. D. Ivanov, T. Augusteijn, S. Brilliant, M. Chadid, J.-G. Cuby, V. Doublier, O. R. Hainaut, E. Le Floc’h, C. Lidman, M. G. Petr-Gotzens, E. Pompei, and L. Vanzi, *AJ* **124**, 417–429 (2002), [astro-ph/0203491](#).
27. L. B. Lucy, *ApJ* **383**, 308–313 (1991).
28. P. A. Mazzali, and L. B. Lucy, *MNRAS* **295**, 428–+ (1998).
29. G. H. Marion, P. Höflich, W. D. Vacca, and J. C. Wheeler, *ApJ* **591**, 316–333 (2003), [astro-ph/0306470](#).